

## Microplasma generation in artificial media and its potential applications\*

Kunihide Tachibana

*Graduate School of Science and Engineering, Ehime University, Matsuyama, Ehime 790-8577, Japan*

*Abstract:* Unlike the generation of uniform plasmas in a large volume, structured plasma comprising microplasmas has attracted increasing scientific and technological interest in recent years. Similarly, the concept of plasma generation in artificial media with gas–gas, gas–liquid, and gas–solid interfaces under intentionally organized and controlled conditions has the potential to open a new field in plasma science and technology. Amongst the subtopics of plasma generation in artificial media, we discuss here those dealing with microplasma jets in flowing gas channels, microdischarges within microbubbles generated in aqueous electrolyte solutions, and discharges in bubbled water and misted air. Our discussion is supported by preliminary results and aims to stimulate future systematic and quantitative investigations.

*Keywords:* gas–gas interface; gas–liquid interface; heterogeneous media; microbubbles; microplasma; mist; structured plasma.

### INTRODUCTION

The growth in the number of applications of non-equilibrium plasmas to materials processing during the last quarter century has created a demand for developing plasma-generation technology, such that it becomes possible to realize uniform plasmas of higher density in larger volumes. However, the issue of dust formation during deposition and etching is recognized as a severe problem that must be addressed. Also, during the past quarter century, the phenomenon of Coulomb-crystal formation of particles trapped in plasmas was discovered, and this phenomenon has since attracted much attention from plasma scientists. Our group has been involved in research into dusty plasma from the very outset [1], and apart from the mechanism of crystal formation itself, we have been particularly interested in the fact that this phenomenon suggests a new idea for artificially structured plasmas, which may create a new area of plasma science. Thus, we have modified our research target to concentrate on the generation of arranged plasma structures via periodic arrays of microplasmas, including the creation of plasma photonic crystals and metamaterials [2]. We have since expanded this concept to include the formulation of a generalized concept of plasma generation in artificially structured heterogeneous media with gas–gas and gas–liquid interfaces.

In this article, we explain the meaning of artificial media. In our interpretation, the term “artificial media” means non-uniform heterogeneous media comprising gas–gas, gas–liquid, or gas–solid mixtures under well-designed and controlled conditions. The example of bubbled water shows that if

---

\*Paper based on a presentation at the 19<sup>th</sup> International Symposium on Plasma Chemistry (ISPC-19), 26–31 July 2009, Bochum, Germany. Other presentations are published in this issue, pp. 1189–1351.

the density and size (distribution) of bubbles contained in water are characterized beforehand, then bubbled water qualifies as an artificial medium. As shown in Fig. 1, we can choose the bubble size to be anywhere from mm to nm. At one extreme in this range, supercritical fluids can be included in the category of artificial media that has nm-sized quantum statistical density fluctuations. Similar to bubbled water, gaseous media with liquid mists may also be included in such a category. Once we succeed in preparing these types of media for the generation of microplasmas, we can create a variety of new concepts for these types of artificial media. In this article, we explain some of our ideas along these lines and present some preliminary experimental results to set the groundwork for more systematic work in the future.

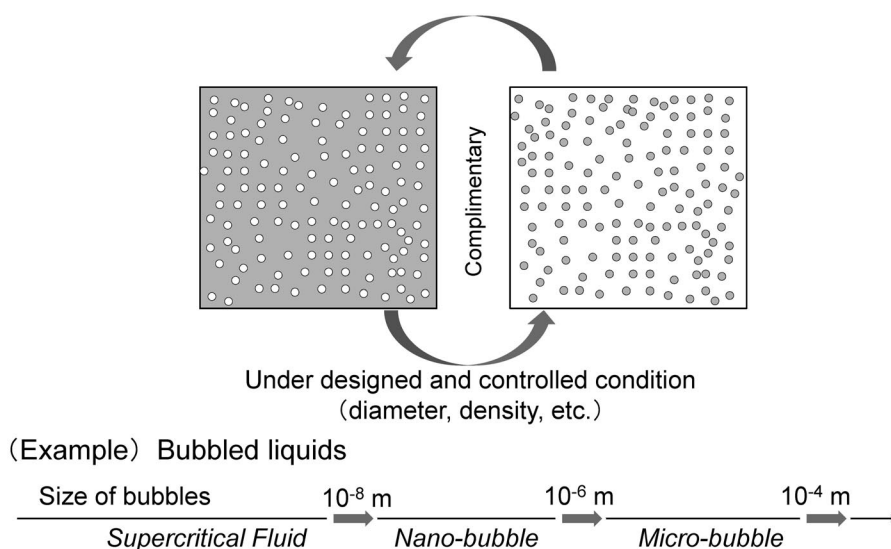


**Fig. 1** Concept of artificial media composed of liquids or gases with bubbles or mists of various sizes.

## STRUCTURED PLASMA COMPOSED OF MICROPLASMAS

All plasmas exhibit specific dielectric properties for high-frequency electromagnetic waves. According to the Drude model, the relative dielectric constant of a plasma,  $\epsilon_p$ , is a function of the frequency  $\omega$  of electromagnetic waves

$$\epsilon_p = 1 - \left( \frac{\omega_{pe}}{\omega} \right)^2 \frac{1}{1 - i(v_m / \omega)} \quad (1)$$

where  $v_m$  is the elastic (momentum transfer) collision frequency of electrons and  $\omega_{pe} = (n_e e^2 / \epsilon_0 m)^{1/2}$  is the electron plasma (angular) frequency, which is a function of the vacuum dielectric constant  $\epsilon_0$ , electron charge  $e$ , mass  $m$ , and density  $n_e$ . We now consider a situation where the medium is composed of a two-dimensional periodic array of columnar microplasmas. In this situation, the dispersion relation between the frequency  $\omega$  and the wave number  $k$  is dependent on the propagation direction of the electromagnetic wave. This allows us to represent  $\epsilon_p$  at an arbitrary position  $\mathbf{r}_{//}$  on the plane perpendicular to the columnar array as the following Fourier expansion with reciprocal lattice vectors  $\mathbf{G}_{//}$  [3]:

$$\epsilon(\mathbf{r}_{//} | \omega) = \sum \hat{\epsilon}(\mathbf{G}_{//}) \exp(i\mathbf{G}_{//} \cdot \mathbf{r}_{//}) \quad (2)$$

where  $\hat{\epsilon}(\mathbf{G}_{//})$  is given by

$$\hat{\epsilon}(\mathbf{G}_{//}) = \epsilon_d - f_v \left[ 1 - \epsilon_d - \frac{\omega_{pe}^2}{\omega(\omega - i\nu_m)} \right] \text{ for } \mathbf{G}_{//} = 0$$

$$= f_v \left[ 1 - \epsilon_d - \frac{\omega_{pe}^2}{\omega(\omega - i\nu_m)} \right] \frac{2J_1(\mathbf{G}_{//}R)}{\mathbf{G}_{//}R} \text{ for } \mathbf{G}_{//} \neq 0$$

Here,  $J_1$  is the first-order Bessel function,  $\epsilon_d$  is the dielectric constant of the medium around the plasma columns of radius  $R$ , and  $f_v$  is the volumetric ratio of the plasma columns. Note that this expression is based on the approximation of superposed plane waves for electromagnetic waves propagating through a periodic structure.

This situation is quite similar to that encountered in photonic crystals in the optical frequency range. However, for artificial media, the frequency shifts toward the sub-terahertz range, because the lattice constant of our periodic structures ranges from the mm to sub-mm scales. This frequency shift is also because of the frequency range of  $\omega_{pe}$  for our microplasmas with  $n_e = 10^{12} \sim 10^{14} \text{ cm}^{-3}$ . As a typical example, we calculated the dispersion relation for a two-dimensional square lattice with a lattice constant  $a$  (Fig. 2a) under the conditions of  $\omega_{pe}a/2\pi c = 0.25$ ,  $\nu_m = 0.5\omega_{pe}$ , and  $f_v = 0.3$  where  $c$  is the speed of light. The resulting dispersion relation is shown in Fig. 2b for the situation where the electric field vector of electromagnetic waves in TE mode is perpendicular to the plasma columns [4]. We note that for propagation along the  $\Gamma$ -X direction, a bandgap appears near  $\omega a/2\pi c = 0.5$ , which is above the cutoff frequency  $\omega_{pe}$ . (The flattened dispersion curves below the cutoff frequency  $\omega_{pe}$  are attributed to the propagation of surface waves around the plasma columns.)

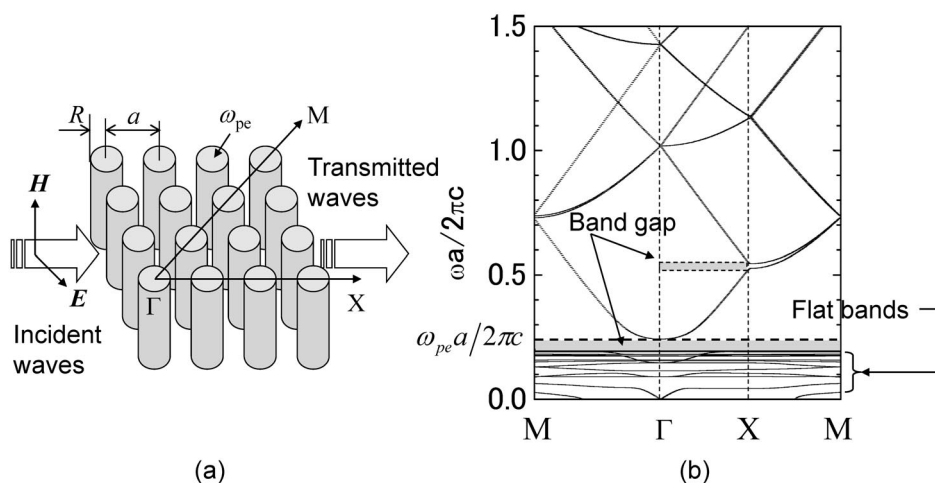


**Fig. 2** (a) Two-dimensional square-lattice array composed of columnar microplasmas and (b) calculated photonic band diagram (i.e., dispersion relation) for electromagnetic waves propagating in TE mode.

To experimentally verify the existence of the bandgap, we constructed a discharge device that consists of a square lattice array of columnar microplasmas with a lattice constant of 2.5 mm, as depicted in Fig. 3a [5]. Each discharge unit has a pair of capillary electrodes with 1-mm bore, 1.6-mm depth, and are separated by a distance of 5 mm. Pulsed bipolar voltage was applied between each pair through a series resistor. The measured relative transmittance  $T$  is plotted in Fig. 3b as a function of  $\omega$ .

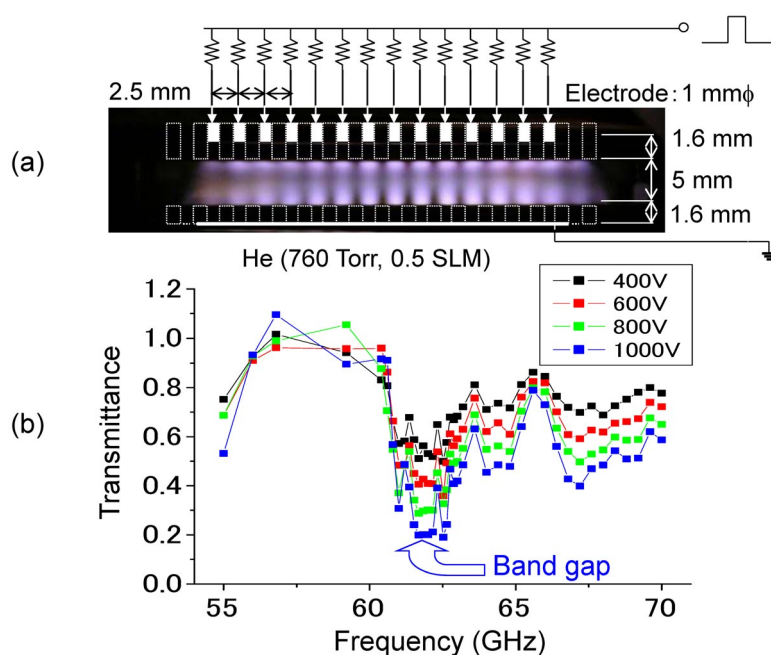


**Fig. 3** (a) Experimental device for two-dimensional square-lattice array of columnar microdischarges driven by pulsed DC discharge and (b) experimental results for transmittance of microwaves plotted as a function of frequency.

A sharp dip is seen near 62 GHz, which corresponds to the bandgap mentioned above. This frequency is primarily determined by the lattice constant and is independent of the applied voltage (i.e., the electron density  $n_e$ ), whereas the depth of the transmittance dip and its width in frequency depend on  $n_e$ . Furthermore, the depth also depends on the number of rows in the array along the propagation direction.

## MICROPLASMA IN MEDIA WITH GAS–GAS INTERFACES

The simplest case of artificial media is the situation with gas–gas interfaces. An interesting example in this category is a microplasma jet generated in a rare-gas (He, Ne, or Ar) flowing channel that is ejected into ambient air [6]. The experimental set-up for this type of jet is illustrated in Fig. 4a. The inner diameter of the glass capillary was 4 mm, and He gas was fed through the bore at a flow rate of 2.8 L/min. A low-frequency (LF), bipolar impulse voltage of 1–20 kHz was applied between the two ring electrodes. We find that a long, thin plasma plume extends into the ambient air along the gas channel. When the jet is observed by a gated intensified charge-coupled device (ICCD) camera with a high temporal resolution, it appears as if a bullet-like bunched plasma is ejected at each cycle of the pulsed discharge and propagates with an apparent speed of a few tens of km/s when positive voltage is applied to the front electrode [7].

Figure 4b shows the spatiotemporal evolution of the density of metastable He\*( $2^3S_1$ ) atoms measured with the set-up illustrated in Fig. 4a. The two-dimensional image of the projected He\* density was obtained from the line-integrated absorption signal by scanning the laser beam in radial and axial directions. The results indicate that the density of noncharged He\* atoms also propagates forward as a bullet at approximately 50 km/s, which is consistent with the ICCD camera observation and the previously reported laser-induced fluorescence measurement of  $N_2^+$  ions [8]. Based on these results and several other experimental results and models [9,10], we attribute the bullet propagation of He atoms to a

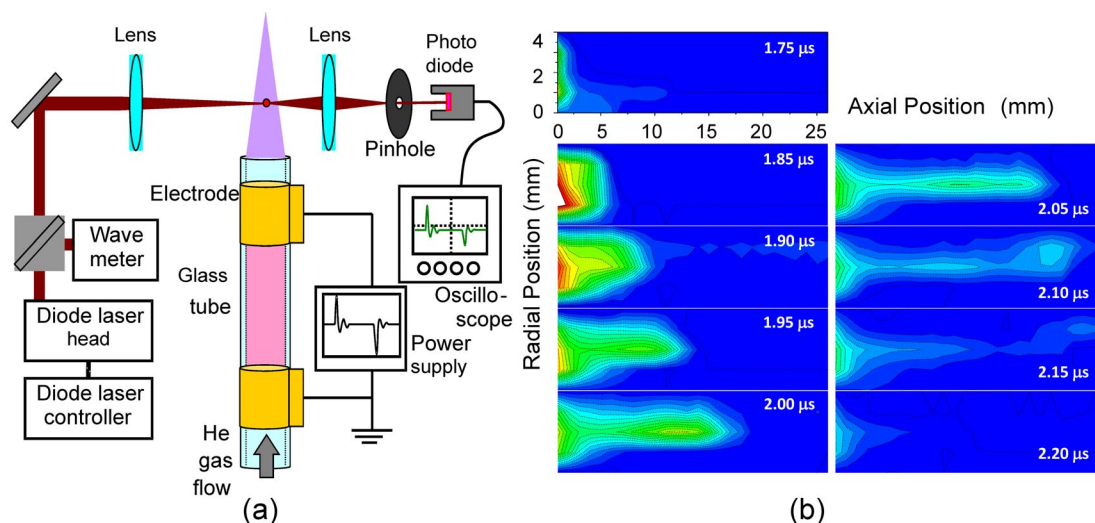


**Fig. 4** (a) Experimental set-up to measure the spatiotemporal behavior of metastable  $\text{He}^*(2^3\text{S}_1)$  atoms in an LF-driven microplasma jet and (b) the results at different times in the positive voltage phase.

phenomenon similar to that which occurs in streamer extension in positive corona discharge. However, the rare-gas channel plays an important role in the straight travel of the ionization front, because in the channel, the electron drift velocity is much faster and the breakdown voltage is lower than in ambient air. It is interesting to see another example in which a DC plasma jet is generated with two gas flows from metallic nozzles crossed at  $90^\circ$  working as electrodes [11]. For the same reasons as just evoked for discharge in the rare-gas channel, the discharge in the crossed channel takes a rectilinear path along the gas flows (as opposed to taking the shortcut path).

We applied this microplasma jet to plasma-enhanced chemical-vapor deposition (CVD) of  $\text{SiO}_2$  films using tetra-ethoxysilane (TEOS) as the source material [12]. We tried three different configurations and found that the best result was obtained with the crossed-beam configuration where the plasma jet is crossed with the vertical source flow, as shown in Fig. 5a. With or without supplying additional ozone, we obtained very large deposition rates (several hundred nm/s), as indicated by the data shown in Fig. 5b. This result may be because during the linear scan of the substrate stage, the interaction time between the active species (provided by the plasma jet) and the source material on the substrate surface is longer in this configuration. However, we find that the deposition rate tends to decrease with decreasing scan speed, which we attribute to accumulated charge on the surface of the deposited film that subsequently causes the plasma jet to spread to avoid the charged area.

This type of plasma jet can easily be integrated to compose a bunched-jet system for processing larger areas. An example of such a design is shown in Fig. 6a, where we used a pair of disc electrodes with  $5 \times 5$  bores at 7-mm pitch separated with each other by 2 cm. The outer and inner diameters of the glass tubes were 3 and 2 mm, respectively. The discharge was driven at a peak bipolar voltage of  $\pm 7$  kV with a repetition frequency of 5 kHz in a total helium gas flow of 3 L/min. We observed plasma plumes evenly prolonged for about 1 cm, as shown in Fig. 6b.

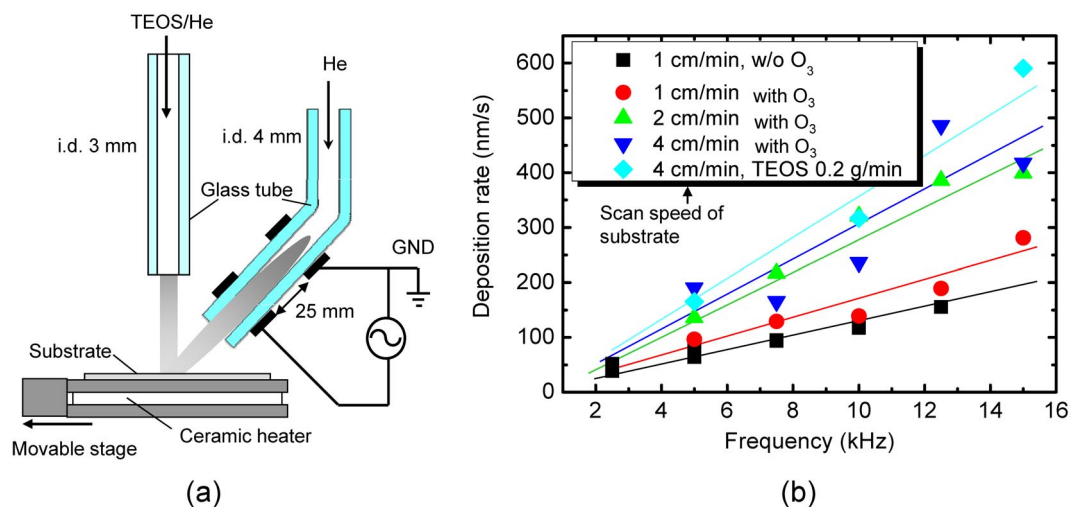


**Fig. 5** (a) Experimental set-up for CVD of SiO<sub>2</sub> films using LF-driven microplasma jet and (b) deposition rate plotted as a function of driving frequency for the experimental conditions noted in the inset.

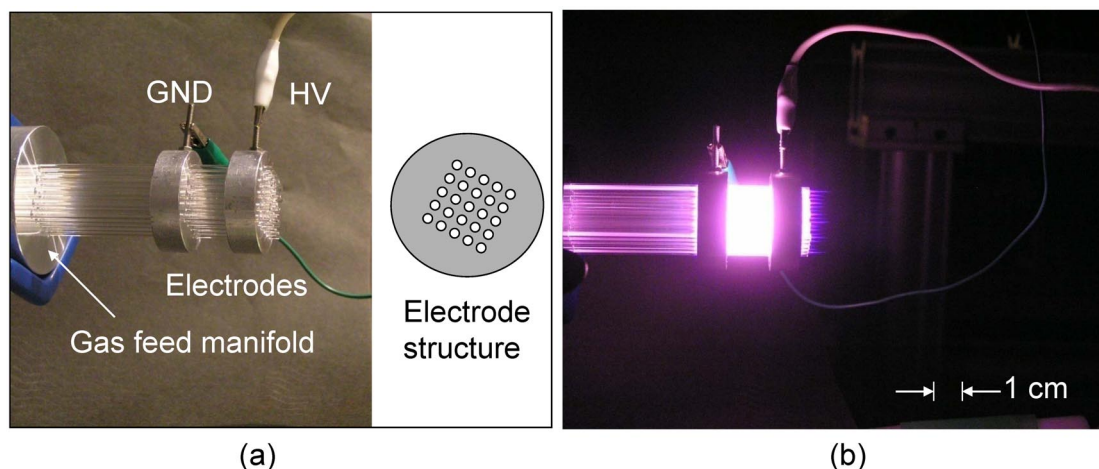


**Fig. 6** (a) Structure of 5 × 5 array of microplasma jets and (b) photo of operation at 5 kHz with a peak applied pulse voltage of 7 kV using He gas flowing at 3 L/min.

## HETEROGENEOUS MEDIA WITH MICROBUBBLES PRODUCED BY ELECTROLYSIS

For the second example of discharge in artificial media, we produced a discharge in microbubbles generated in water by electrolysis with addition of Na<sub>2</sub>CO<sub>3</sub> (3 wt %) [13]. A schematic of the experimental apparatus is shown in Fig. 7a. The electrode had a fabric structure with an insulated metal wire serving as the warp and a bare metal wire serving as the weft. The electrode was positioned a few cm from the third electrode, and the electrodes were connected with a DC power supply for the electrolysis. The bubbles were held on the surface of the fabric electrode.

By applying an AC voltage of approximately 3 kV peak-to-peak between the warp and the weft, we find that the discharge occurs inside the microbubbles, as seen in Fig. 7b. The advantages of this configuration are that the electrode structure not only allows low-voltage ignition of the atmospheric-pressure discharge in hydrogen or oxygen microbubbles, but is also effective in producing and holding

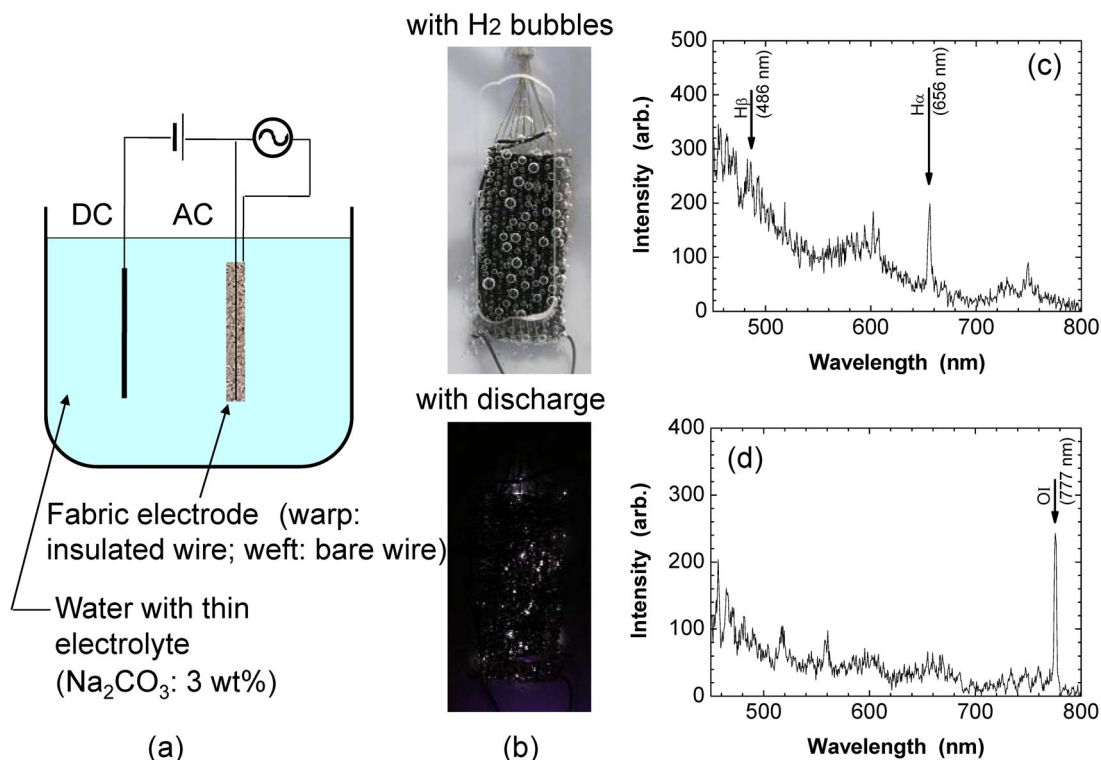


**Fig. 7** (a) Set-up for underwater discharge in microbubbles generated by electrolysis in electrolyte solution, (b) photos of fabric electrode covered with  $\text{H}_2$  bubbles (b, upper panel) and the discharge in bubbles (b, lower panel), and observed emission spectra in (c)  $\text{H}_2$  bubbles and (d)  $\text{O}_2$  bubbles.

bubbles on its surface. We verified that the reactive species were generated by observing optical emission from the resulting microplasmas, as shown in Fig. 7c. The transport of these species into the solution was monitored by the change in the pH of the solution, as reported previously [13].

To make this system more practical for an application such as sterilization and water purification, a dynamic cycle should be established for the bubble generation, the microdischarge generation, and the release of the active species into the solution by breaking bubbles with discharge or forced liquid flow. We have tried the reduction of  $\text{CO}_2$  in aqueous solution by the same principle using a modified system and successfully observed  $\text{CO}$  as the product [14].

## HETEROGENEOUS MEDIA GENERATED BY FORCED INJECTION OF BUBBLES IN WATER

As the third example of artificial media, we introduced micro air bubbles into water with the aim of producing discharge in the mixture. We used an open-end insulated wire as the anode and a metal plate placed at the bottom of the vessel as the cathode. The variation in the appearance of the discharge, shown in Fig. 8a, was observed at various bubble concentrations. For a certain bubble concentration, the measured ignition and sustain voltages with and without bubbles is plotted in Fig. 8b as a function of the discharge repetition frequency. It is seen that both the ignition and sustain voltages in the bubbled water are much lower than those in the pristine water. The decreasing tendency seen in the pristine water with increasing repetition frequency is attributed to the generation of bubbles by the discharge itself.

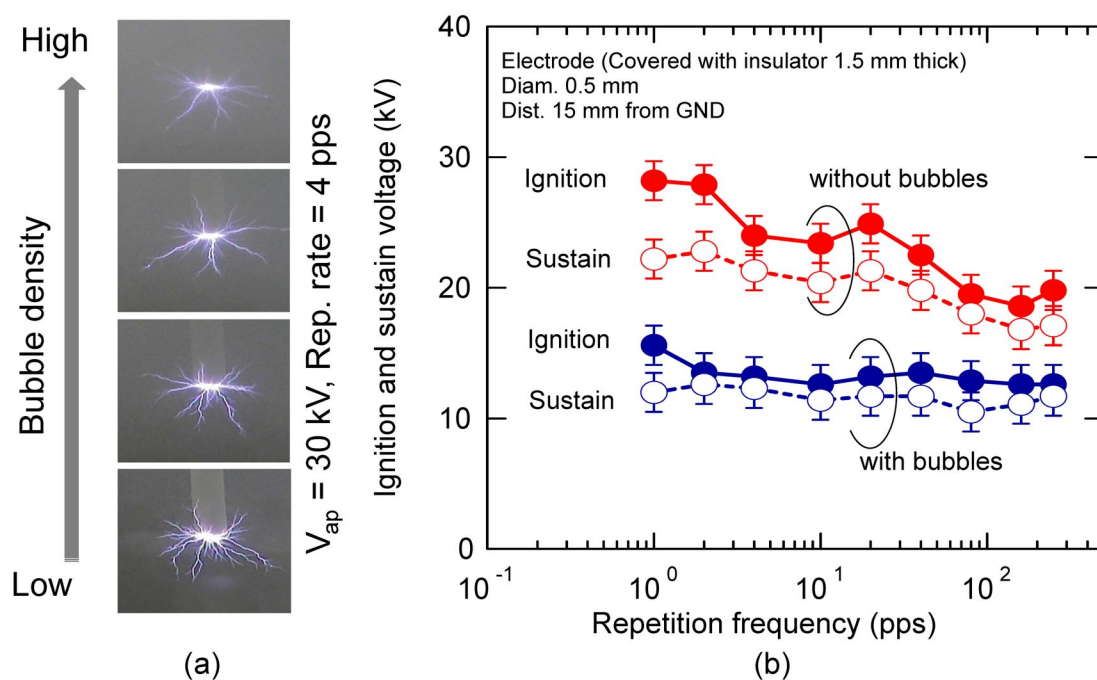


**Fig. 8** (a) Photos of corona discharge in the point-plane configuration in bubbled water at various bubble concentrations, and (b) ignition and sustain voltages plotted as a function of the repetition frequency.

However, this situation does not fit within our category of artificial media, because the bubbles are not introduced under controlled conditions, and their size and density are not as yet specified. We are currently preparing the measurement of these parameters using dynamic light scattering with an Nd-YAG laser in which the temporal scattered light signal from the laser focus point is detected using a photon-counting technique and analyzed for its self-correlation. As a preliminary trial, we used a commercial system to measure a small volume of water and observed submicron bubbles that persisted after the disappearance of visible bubbles. The presence of these small bubbles may not be effective in decreasing the ignition voltage because the volumetric concentration ratio is too small. However, we expect these bubbles to have another effect on the electrical and chemical properties of the medium because of their electronegative tendency. In future experiments, we also plan to introduce gases other than air.

## HETEROGENEOUS MEDIA GENERATED BY FORCED INJECTION OF MIST IN AIR

As the final example of artificial media, we generated discharge in air admixed with microliquid particles in the form of mist. Figure 9 shows the experimental set-up employed, in which the mist of material solution was generated by ultrasonic vibration through a polyethylene sheet and transferred by carrier gas fed into the evaporation chamber. Next, the mist was transported through a silicon rubber tube to the discharge electrode assembly shown in Figs. 9b,c, which was composed of double layers of insulated metal meshes [15]. The discharge was ignited via a dielectric barrier discharge (DBD) scheme by applying a bipolar pulsed voltage between the mesh electrodes, so that the DBD was composed of many microdischarges filling all through-holes. Excellent uniformity and stability were obtained over the entire, 5-cm-diameter opening area (Fig. 9d), even with an admixture of methanol mist.

We also attempted using a typical parallel-plate DBD system, but the discharge became filamentary upon admixture of mist. For a variety of practical uses, this integrated microplasma system can eas-

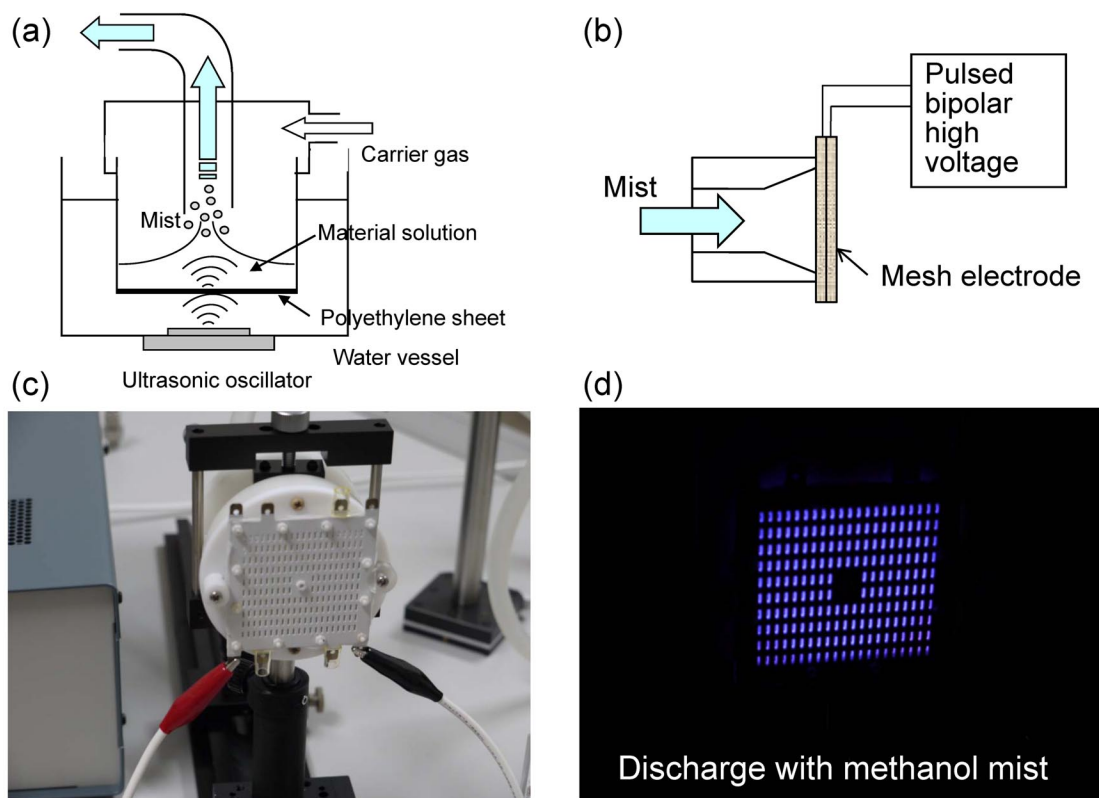


**Fig. 9** Schemes of (a) mist generation and transport parts and (b) experimental set-up for discharge in misted air, and photos of (c) mesh-electrode assembly and (d) discharge image in air containing methanol mist.

ily be scaled up to a fairly large size without losing the uniformity and stability of the plasma. However, we need to quantitatively characterize the size and density of mist using, for example, light-scattering and/or ellipsometric techniques [16] to ensure that mist-containing gases form appropriate artificial media.

## CONCLUDING REMARKS

In generalizing the concept of artificial media, which consists of two-phase mixtures of gases and liquids, it is necessary to systematically change the size and volumetric ratio of bubbles or mists in a controlled manner. In addition, proper diagnostic methods for characterizing the size and density of the bubbles or mists should be established to cover a wide range of sizes, from nm to mm. Once these types of well-defined, two-phase mixed media can be routinely prepared for the generation of plasmas, the systematic research of plasmas using these media will create a new field of plasma science. Other interesting media that may be categorized in this family of two-phase media include supercritical fluids as mentioned above and any liquids under negative pressure in which spontaneous cavitations are induced.

Finally, we note that to mirror theoretical approaches, these experimental approaches should be performed to the best possible extent in simplified and well-defined model systems. In this way, a variety of applied technologies may be developed on the basis of scientific approach illustrated in Fig. 10.

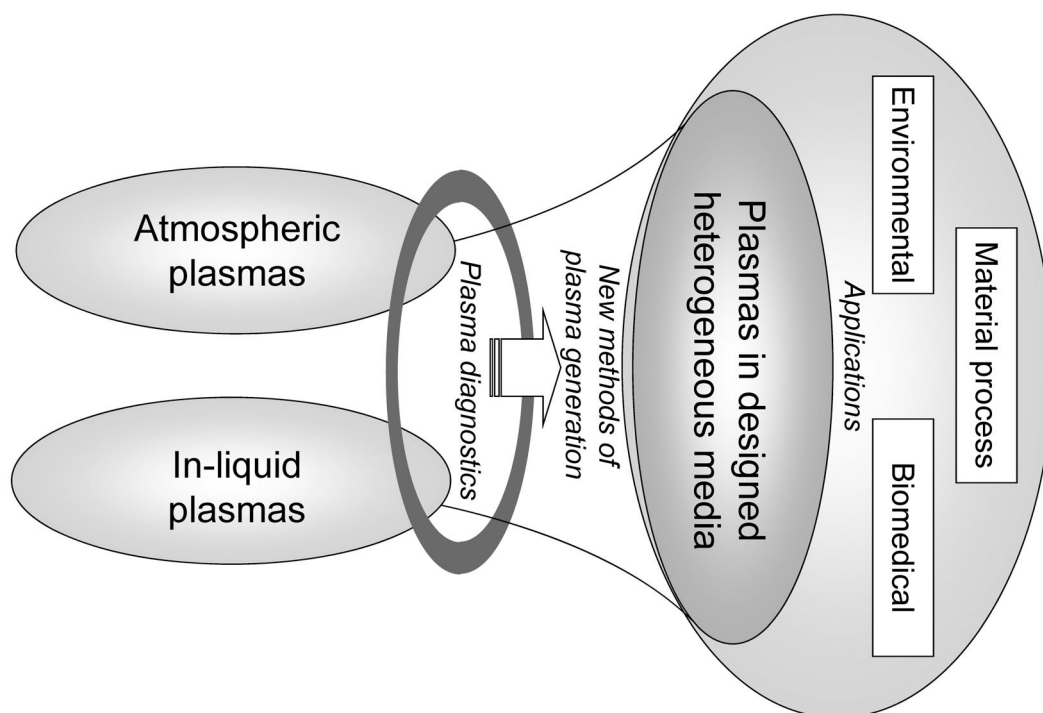


**Fig. 10** Concept for creation of a new field of plasma science and technology by merging two different research categories into the single category of research into plasmas in artificial media that consist of two-phase mixtures.

## ACKNOWLEDGMENTS

The author acknowledges O. Sakai, T. Shirafuji, and K. Urabe for their collaborations in the experimental parts. This work is partially supported by a Grant-in-Aid for Scientific Research from the Ministry of Education, Culture, Sports, Science, and Technology (Japan).

## REFERENCES

1. Y. Hayashi, K. Tachibana. *Jpn. J. Appl. Phys.* **33**, L804 (1994).
2. O. Sakai, T. Sakaguchi, T. Naito, D.-S. Lee, K. Tachibana. *Plasma Phys. Control. Fusion* **49**, B453 (2007).
3. V. Kuzmiak, A. A. Maradudin. *Phys. Rev. B* **55**, 7427 (1997).
4. O. Sakai, T. Sakaguchi, K. Tachibana. *J. Appl. Phys.* **101**, 073304 (2007).
5. T. Sakaguchi, O. Sakai, K. Tachibana. *J. Appl. Phys.* **101**, 073305 (2007).
6. M. Teschke, J. Kedzierski, E. G. Finantu-Dinu, D. Korzec, J. Engemann. *IEEE Trans. Plasma Sci.* **33**, 310 (2005).
7. B. L. Sands, B. N. Ganguly, K. Tachibana. *IEEE Trans. Plasma Sci.* **36**, 956 (2008).
8. K. Urabe, Y. Ito, K. Tachibana, B. N. Ganguly. *Appl. Phys. Expr.* **1**, 066004 (2008).
9. X.-P. Lu, M. Laroussi. *J. Appl. Phys.* **100**, 063302 (2006).
10. G. V. Naidis. *Proc. 19<sup>th</sup> Int. Symposium on Plasma Chemistry*, O3.01, Bochum, Germany (2009).
11. N. Shirai, S. Ibuka, S. Ishii. *IEEE Trans. Plasma Sci.* **36**, 960 (2008).
12. Y. Ito, K. Urabe, N. Takano, K. Tachibana. *Appl. Phys. Expr.* **1**, 067009 (2008).
13. O. Sakai, M. Kimura, T. Shirafuji, K. Tachibana. *Appl. Phys. Lett.* **93**, 231501 (2008).

14. O. Sakai, T. Morita, N. Sano, T. Shirafuji, T. Nozaki, K. Tachibana. *J. Phys. D: Appl. Phys.* **42**, 202004 (2009).
15. O. Sakai, Y. Kishimoto, K. Tachibana. *J. Phys. D: Appl. Phys.* **38**, 431 (2005).
16. Y. Hayashi, K. Tachibana. *Jpn. J. Appl. Phys. Part 2* **33**, L476 (1994).